Acta Pharmaceutica Sinica B 2022;12(4):1624–1635

Chinese Pharmaceutical Association
Institute of Materia Medica, Chinese Academy of Medical Sciences

Acta Pharmaceutica Sinica B

www.elsevier.com/locate/apsb
www.sciencedirect.com

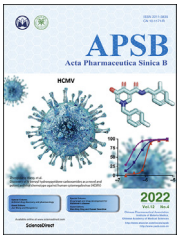

ORIGINAL ARTICLE

Suppressing fatty acid synthase by type I interferon and chemical inhibitors as a broad spectrum anti-viral strategy against SARS-CoV-2

Saba R. Aliyari[a,†], Amir Ali Ghaffari[a,†], Olivier Pernet[a,b], Kislay Parvatiyar[a], Yao Wang[a], Hoda Gerami[a], Ann-Jay Tong[a], Laurent Vergnes[c], Armin Takallou[a], Adel Zhang[a], Xiaochao Wei[d], Linda D. Chilin[e], Yuntao Wu[e], Clay F. Semenkovich[d,f], Karen Reue[c], Stephen T. Smale[a], Benhur Lee[a], Genhong Cheng[a,*]

[a]*Department of Microbiology, Immunology and Molecular Genetics, University of California, Los Angeles, CA 90095, USA*
[b]*EnViro International Laboratories, Los Angeles, CA 90077, USA*
[c]*Department of Human Genetics, David Geffen School of Medicine, University of California, Los Angeles, CA 90095, USA*
[d]*Division of Endocrinology, Metabolism and Lipid Research, Washington University School of Medicine, St. Louis, MO 63110, USA*
[e]*Center for Infectious Disease Research, School of Systems Biology, George Mason University Manassas, VA 20110, USA*
[f]*Diabetic Cardiovascular Disease Center, Washington, University School of Medicine, St. Louis, MO 63110, USA*

Received 20 November 2021; received in revised form 27 January 2022; accepted 8 February 2022

KEY WORDS

Fatty acid synthase;
FASN;
IFN-I;
SARS-CoV-2;
COVID-19;
C75;

Abstract SARS-CoV-2 is an emerging viral pathogen and a major global public health challenge since December of 2019, with limited effective treatments throughout the pandemic. As part of the innate immune response to viral infection, type I interferons (IFN-I) trigger a signaling cascade that culminates in the activation of hundreds of genes, known as interferon stimulated genes (ISGs), that collectively foster an antiviral state. We report here the identification of a group of type I interferon suppressed genes, including fatty acid synthase (FASN), which are involved in lipid metabolism. Overexpression of FASN or the addition of its downstream product, palmitate, increased viral infection while knockout or

*Corresponding author. Tel.:+1 310 825 8896; fax: +1 310 206 5553.
E-mail address: Gcheng@mednet.ucla.edu (Genhong Cheng).
†These authors made equal contributions to this work.
Peer review under responsibility of Chinese Pharmaceutical Association and Institute of Materia Medica, Chinese Academy of Medical Sciences.

https://doi.org/10.1016/j.apsb.2022.02.019

Cerulenin;
TVB-3166

knockdown of FASN reduced infection. More importantly, pharmacological inhibitors of FASN effectively blocked infections with a broad range of viruses, including SARS-CoV-2 and its variants of concern. Thus, our studies not only suggest that downregulation of metabolic genes may present an antiviral strategy by type I interferon, but they also introduce the potential for FASN inhibitors to have a therapeutic application in combating emerging infectious diseases such as COVID-19.

1. Introduction

Severe acute respiratory syndrome coronavirus-2 (SARS-CoV-2) is an emerging, positive strand RNA virus from the Coronaviridae family[1]. As the etiological agent of the coronavirus disease 2019 (COVID-19) pandemic, SARS-CoV-2 has become one of the most challenging public health threats faced in decades, with a major sociological and economic impact[2]. Despite drastic global efforts to reduce the spread of infection and develop novel treatments and vaccines, the pandemic is to date still uncontrolled, with over 200 million cases and 4.5 million deaths by the end of August, 2021[3]. While the classic presentation of COVID-19 is a respiratory syndrome with a high case-fatality rate, particularly in seniors and those with certain pre-existing health conditions, SARS-CoV-2 infection can also trigger an autoimmune multi-systemic inflammatory disorder, particularly in children[4]. To combat novel viruses such as SARS-CoV-2 and future emerging viral infections to which we have no specific therapies, it is critical that we develop agents with broad antiviral effects. Investigating innate immune responses, which have evolved to protect the host against multiple types of viral infections, can help us to identify novel strategies to boost or replicate these broad defenses.

The innate immune system provides a critical first line of defense against invading pathogens, including those of viral origin. Utilizing select germ line encoded pattern recognition receptors (PRRs), cells of the innate immune system detect pathogen-associated molecular patterns (PAMPs), which are highly invariable structures of microbial origin, elicits an antiviral gene program known as the host type I interferon (IFN-I) response, characterized by the induction of IFN-I and ISGs. Viral RNA and DNA species generated during replicative cycles serve as PAMPs and are typically detected in the cytosol by nucleic acid sensing PRRs[5–9]. Recognition of viral RNA species by the RIG-I like family of RNA sensors, or viral DNA species by the cGAS, DDX41, or IFI16 DNA sensors, triggers the activation of the innate antiviral IFN-I response[10–12]. Microbial nucleic acids detected on the cell surface or in endosomal compartments can also activate the host IFN-I response *via* membrane bound PRRs, such as Toll-like receptors (TLRs) 3, 7, 8, and 9. TLR4[10,13,14] which detects lipid A and lipopolysaccharide (LPS) derived from the cell walls of gram-negative bacteria, is also known to trigger the IFN-I response[15].

A central paradigm of innate antiviral immunity is that IFN-I, namely IFNα and IFNβ, play essential roles in fostering an antiviral state[16,17]. Operating primarily in a paracrine fashion, these cytokines bind to the IFNα/β receptor (IFNAR) on neighboring cells to instigate a Janus kinase-signal transducer and activator of transcription (JAK−STAT) signaling cascade, which culminates in the up-regulation of nearly 300 ISGs[18,19], which directly target viral components or orchestrate cellular processes that lead to the inhibition of virus replication and spread[20]. Alternatively, certain genes are downregulated by IFNα, β, and γ[21] as a mechanism to control viral infections[22]. Modulation of enzymes involved in the fatty acid synthesis pathway plays a pivotal role in the regulation of infection for many viruses, including human cytomegalovirus (HCMV)[23], Kaposi sarcoma-associated herpesvirus (KSHV)[24], dengue virus (DENV)[25–27], chikungunya virus[28], Rotavirus[29], and hepatitis C virus (HCV)[30–32]. Utilizing an RNA sequencing (RNAseq) approach, we comparatively evaluated gene expression profiles between wild type (WT) and *Ifnar*-deficient immune cells after PRR stimulation, and identified fatty acid synthase (*Fasn*) as an IFN-I suppressed gene that is required for optimal viral infectivity. Our results also reveal that fatty acid synthase (FASN) plays an essential role in mediating viral entry, and that inhibition of FASN by pharmacological compounds represents a novel broad antiviral strategy against a wild range of viruses, including SARS-CoV-2.

2. Materials and methods

2.1. Animals

The experiments were performed in accordance with the Institutional Animal Care and Use Committee guidelines from the University of California Los Angeles (CA, USA). Age and sex matched, 6- to 10-week-old mice were used for all experiments. C57Bl/6 and *Stat*$^{-/-}$ mice were purchased from Jackson laboratories. LysM-*Fasn* mice were a kind gift from Dr. Semenkovich lab and generated as described[33]. *Tlr3*$^{-/-}$/*Cardif*$^{-/-}$ double knockout mice were crossed in our laboratory as described previously[34].

2.2. Viruses

Dr. Glen Barber (University of Miami, Florida, CA, USA) provided VSV-GFP. MHV68-Luc was provided by Dr. Ren Sun in UCLA (CA, USA). HSV-1, HSV-1 KOS Strain expressing GFP in frame with the ICP0 protein between amino acids 10^4 and 10^5 was a kind gift of Dr. William Halford (Southern Illinois University School of Medicine, IL, USA). HSV-1 expressing both GFP and luciferase reporter was a kind gift from Dr. Chunfu Zheng[35]. The recombinant SARS-CoV-2 (icSARS-CoV-2-mNG) expressing mNeonGreen[36] was a kind gift from World Reference Center for Emerging Viruses and Arboviruses (WRCEVA), Department of Microbiology and Immunology, University of Texas Medical Branch through an MTA. SARS-CoV-2 variant of concerns SARS-CoV-2-α (SARS-CoV-2, Isolate hCoV-19/USA/OR-OHSU-PHL00037/2021-B.1.1.7), SARS-CoV-2-β (SARS-CoV-2, Isolate hCoV-19/USA/MD-HP01542/2021B.1.351), SARS-CoV-2-γ (SARS-CoV-2,

Isolate hCoV-19/Japan/TY7-503/2021-P.1 or 20J/501Y.V3), and SARS-CoV-2-δ (SARS-CoV-2, Isolate hCoV-19/USA/PHC658/2021-B.1.617.2) were provided by Dr. Vaithilingarajai Arumugaswami who obtained them from the BEI resources.

2.3. Reagents

Luciferase activity was measured using firefly luciferase substrate kit (Promega). *Fasn* expression plasmids were obtained from Invitrogen, and transfected using Lipofectamine 2000 from Invitrogen according to their protocol. Lipofectamine 2000 was also used for polyI:C transfection (1:1 ratio) in MEFs. Silencer select validated siRNAs were purchased from Ambion and transfected using RNAiMAX transfection reagent from Promega according to their protocol. C75 and cerulenin were from Cayman and EGCG and TVB-3166 were from Sigma. TLR ligands were purchased from Invivogen. All *in vitro* experiments were repeated at least three times with biological triplicates within each experiment.

2.4. Primary cells and cell lines

A549, Vero, HEK 293 T, and RAW264.7 cells were grown in standard Dulbecco's modified Eagle's medium (DMEM; ThermoFisher) with 10% FBS, 1% penicillin−streptomycin (GIBCO). Bone marrow-derived macrophages (BMDMs) were harvested from 6−8-week C57B/L6 mice (Jackson Labs) and differentiated in DMEM+10%FBS+2%MCSF for 7 days. Media was replaced every other day, and on Day 7 cells were stimulated with ligands. Mouse embryonic-derived fibroblasts (MEF) were derived by skinning the tails of mice and incubating them directly in culture dishes in DMEM with 10% FBS. Cells were scraped and re-plated after 7 days. Vero-E6 and Huh7.5 cell lines were purchased from ATCC, and Hela-ACE2 cells, a kind gift from Dr. Guangxiang Luo from UAB, were cultured in DMEM supplemented with 10% FBS (HyClone), and 1% penicillin−streptomycin (Gibco) at 37 °C in a 5% CO_2 humidified atmosphere.

2.5. RNA isolation and RNAseq

5×10^5 BMDMs derived from wild type (C57BL/6) and *Ifnar*$^{-/-}$ mice were stimulated with Lipid A (100 ng/mL, Sigma) or saline control for 6 h. Cells were harvested in Trizol (Invitrogen) and RNA was isolated by using Qiagen RNeasy Mini Kit (Qiagen) according to manufacturer's protocol. Polyadenylated RNA was purified from 10 μg of total RNA using the Micro-polyA Purist kit (Ambion) according to manufacturer's protocol. Prior to cDNA library construction for RNA-Seq analyses, RNA was quantified and assessed for quality (RNA Integrity Value) using an Agilent 2100 Bioanalyzer (Agilent Technology, Santa Clara, CA, USA). cDNA libraries were constructed as previously described using 100 ng of PolyA + purified RNA as input[37,38]. All sample sequencing was performed by the Broad Stem Cell Research Center High Throughput Sequencing Core at UCLA on the Illumina HiSeq 2000 with a single end sequencing length of 50 nt. Sequence reads from cDNA libraries were aligned to the mouse genome build NCBI37/mm9 using Tophat[39]. Alignments were restricted to uniquely mapped reads, with two possible mismatches permitted. RPKM (reads per kilobase per million) values were calculated for mm9 Refseq genes using Seqmonk (http://www.bioinformatics.babraham.ac.uk/projects/seqmonk/). RNAseq data is available at the NCBI GEO database under accession number GSE38892.

2.6. VSV, HSV-1, MHV68, and SARS-CoV-2 viral plaque assay

HEK 293 T cells were infected with VSV-GFP at multiplicity of infection (MOI) of 0.01 for 1 h and the media was replaced with the fresh one. Approximately 150 μL of supernatants were collected at various time points between 8 and 16 h-post infection (hpi) for plaque assay. For HSV-1 and MHV68, 0.25 MOI was used for infection (unless otherwise specified) and supernatants were collected at 24 hpi. Plaque assays were done on Vero cells in 12-well plates at 2×10^5, 5×10^4 and 2×10^4 cells per well for VSV, HSV-1, and MHV68, respectively. Supernatants from infected cells were serially diluted and cells were infected for 1 h. The cells were then covered with growth medium containing low-melting point agarose. Plaques were stained with crystal violet 0.5% (*w*/*v*) in 4% PFA (*v*/*v*) and were counted after 16 h, 3, and 6 days for VSV, HSV-1, and MHV68, respectively.

Hela cells expressing ACE2 (Hela-ACE-2) were used for SARS-CoV-2 plaque assay. Briefly, media were removed from the confluent mono-layer of Hela-ACE-2 cells followed by infecting cells with the serially diluted virus and incubated for 1 h at 37 °C in a 5% CO_2 humidified atmosphere. Cells were then washed with 1 × PBS and then were covered with agarose-overlay. At 72 hpi, the agarose-overlay was removed, cells were washed with 1 × PBS, fixed by 4% PFA for 1 h, and plaques were developed by staining cells with crystal violet containing 1% PFA for 30 min.

2.7. SARS-CoV-2 viral RNA copy number assay

200 μL of the supernatant was harvested from cells infected with SARS-CoV-2 and mixed with equal volume of lysis buffer provided in the high pure viral RNA kit (Invitrogen) and RNA was extracted according to the kit's instructions. The eluted RNA was subjected to RT-qPCR by using the One Step TB Green PrimeScript RT-qPCR Kit II (Takara) and specific primers targeting the SARS-CoV-2 nucleocapsid protein (NP):

Forward, 5′-TAATCAGACAAGGAACTGATTA-3′;

Reverse, 5′-CGAAGGTGTGACTTCCATG-3′.

RT-qPCR cycling conditions were 42 °C for 5 min, 95 °C for 10 s, and 40 cycles of 95 °C for 5 s, followed by 60 °C for 30 s.

All the SARS-CoV-2 based experiments were performed at the UCLA BSL3 facility.

2.8. VSV-G pseudotyped VSV-G luciferase pseudovirus production

VSV-G pseudotyped VSV-G luciferase pseudovirus (VSVΔG-Luc/G) was generated by methods previously described and concentrated by ultracentifugation on 20% sucrose cushion[40]. The VLPs were resuspended in NTE buffer (100 mmol/L NaCl; 10 mmol/L Tris-HCl, pH 7.5; 1 mmol/L EDTA) and stored in −80 °C. The concentrations used to generate linear range of luciferase signal were determined empirically.

The assembly of hybrid alphavirus SARS-CoV-2 pseudovirus and its variants were described previously[41]. Briefly, Ha-CoV-2 particles were assembled by cotransfection of HEK 293 T cells in 10 cm dish with 2.5 μg of each of the SARS-CoV-2 structural protein expression vectors (S, N, E, M) and 10 μg of Ha-CoV-2(Luc). Particles were harvested at 48 h post-cotransfection, filtered through a 0.45 μm filter. Ha-CoV-2 particles were used

to infect HEK293T-ACE2/TEMPRESS2 cells (a gift from Virongy LLC, Manassas, VA, USA). For C75 inhibition assay, 2.5×10^4 HEK293T-ACE2/TEMPRESS2 cells in each well of 96 well plates were pre-treated with serially diluted C75 for 1 h, cells were infected with Ha-CoV-2(Luc) or its variants of concern for 18 h. Cells were lysed in Luciferase Assay Lysis Buffer (Promega) for luciferase assays using GloMax Discover Microplate Reader (Promega).

2.9. VSVG/βlaM production

A previously described construct encoding Nipah-M1 fused with β-lactamase (βlaM) was used to package inside VSV-G[42]. HEK 293 T cells were transfected with constructs encoding βlaM and VSV-G or βlaM alone (bald) at 3:1 ratio in 10 cm dishes by polyethylenimine (PEI) transfection reagent. The viral supernatants were collected, clarified, and concentrated by ultracentrifugation at $> 75{,}000 \times g$ on 20% sucrose cushion and the pellet was resuspended in NTE buffer.

2.10. RT-qPCR

Cells were collected in Trizol and RNA was isolated by standard isopropanol precipitation. RNA was quantified and 1 μg of RNA was reversed transcribed using iScript (BioRad) according to the manufacturer's instructions with random hexamer as primers. RT-qPCR analysis was done using the iCycler thermocycler (Bio-Rad). RT-qPCR was conducted in a final volume of 20 μL. Amplification conditions were: 95 °C (3 min), 40 cycles of 95 °C (20 s), 55 °C (30 s), 72 °C (20 s). Expression values were normalized to ribosomal RNA L32 and fold induction was normalized to untreated control.

2.11. Viral RNA detection

For detection of VSV genomic RNA, cells infected with VSV were collected in Trizol and RNA was isolated and reverse transcribed with VSV specific primer N1-5′-GATAGTACCGGAGGATTGACGACTA using Superscript II (Invitrogen) according to manufacturer's protocol. Real time RT-qPCR with Taqman probe with conditions described above. VSV fwd: 5′-GATAGTACCGGAGGATTGACGACTA-3′;

VSV rev: 5′-TCAAACCATCCGAGCCATTC-3′;

VSV probe: 5′-(FAM)-TGCACCGCCACAAGGCAGAGA-(TAMRA)-3′.

For detection of SARS-CoV-2 genomic RNA, the below primers targeting SARS-CoV-2 nucleo capsidprotein (NP) were used:

NP-fwd, 5′-TAATCAGACAAGGAACTGATTA-3′;

NP-rev, 5′-CGAAGGTGTGACTTCCATG-3′.

2.12. MHV68 mouse infections

C57BL/6 mice (6−8 weeks) were purchased from Jackson. Mice were first anesthetized by intraperitoneal (i.p.) injection with 200 mg/kg ketamine, 4 mg/kg xylazine in PBS and shaved. MHV68 (500 pfu) in 200 μL of PBS was administered by i.p. On day three following infection, mice were imaged using the *in vivo* imaging system (IVIS, Xenogen). Briefly, mice were anesthetized with isoflurane and administered 3 mg D-luciferin/mouse by i.p. Injection prior to imaging. Grayscale photographs and color images of imaged mice were superimposed with LivingImage (Xenogen) and Igor (Wavemetrics) programs, similar to that previously described[20]. The mice were imaged on dorsal, ventral, right, and left side until the maximal luminescence has passed.

2.13. Generation of *FASN*$^{-/-}$ A549 cells using CRISPR/Cas9 technology

FASN knockout A549 cell line was obtained using CRISPR/Cas9 system. The target sequences of the two sgRNAs (GCCGG CATGTCCGGGAAGCTGC and CCAGACGCCAGTGTGTGT TCCT) flanked by BsaI restriction site were cloned into px601 plasmid (Addgene) expressing *Staphylococcus aureus* Cas9 (*Sa*Cas9) together with a complete gRNA. Plasmids were then transfected into A549 cells 5 times using lipofectamin 2000 (invitrogene), every three days. The *FASN*$^{-/-}$ single clone was selected by serial dilution and confirmed by Western blotting.

2.14. Identification of CC_{50} and IC_{50} values

Twenty hours prior to the cytotoxicity assay, 8×10^3 Hela-ACE-2, 1.2×10^4 Huh 7.5 and 1.2×10^4 Vero-E6 cells were seeded in 96 Well White/Clear Bottom Plate, TC Surface (Thermo Fisher). Cells were treated with 2-fold serial dilutions (100−1.5 μmol/L) of C75, (160−2.5 μmol/L) of cerulenin, and (160−2.5 μmol/L) of TVB-3166 for 20 h. The cell viability was determined by using Cell Titer-Glo® luminescent cell viability assay (Promega). IC_{50} and CC_{50} values were calculated by non-linear regression analysis using GraphPad 5.

2.15. Statistical analysis

The data were analyzed with unpaired student *t*-test. by Prism software (GraphPad). All of the data are shown as mean + standard deviation (SD) or mean ± standard error of mean (SEM) from three independent experiments. $^*P \leq 0.05$, $^{**}P \leq 0.01$, $^{***}P \leq 0.001$.

3. Results

3.1. FASN is an IFN-I suppressed gene

To identify genes that are downregulated by IFN-I during PRR signaling, WT and *Ifnar*$^{-/-}$ bone marrow-derived macrophages (BMDMs) were stimulated with Lipid A, a TLR4 agonist, and subjected to RNAseq analysis. Ingenuity software profiling of canonical pathways revealed that multiple genes in fatty acid biosynthesis and glycerophospholipid metabolism were downregulated in WT BMDMs, but upregulated in *Ifnar*$^{-/-}$ BMDMs (Fig. 1A and B). Accordingly, expression of the gene encoding fatty acid synthase (*Fasn*) was confirmed by RT-qPCR to be elevated in *Ifnar*$^{-/-}$ BMDMs and reduced in WT BMDMs, consistent with a decrease in FASN protein levels upon TLR4 stimulation (Fig. 1C and D). Cytosolic PRRs that detect viral nucleic acids to activate the IFN-I response also downregulated *Fasn*, as BMDMs stimulated with the double stranded (ds) RNA mimetic, polyI:C (pI:C), or dsDNA (poly dA:dT), displayed a marked reduction in *Fasn* gene expression (Fig. 1E and Supporting Information Fig. S1A). *Fasn* was also suppressed by IFN-I activating ligands in murine embryonic fibroblasts (MEFs) as well as A549 human lung epithelial cells, suggesting that *Fasn* downregulation is not restricted to immune cells (Fig. S1B and S1C). TLR4 and cytosolic nucleic acid sensing

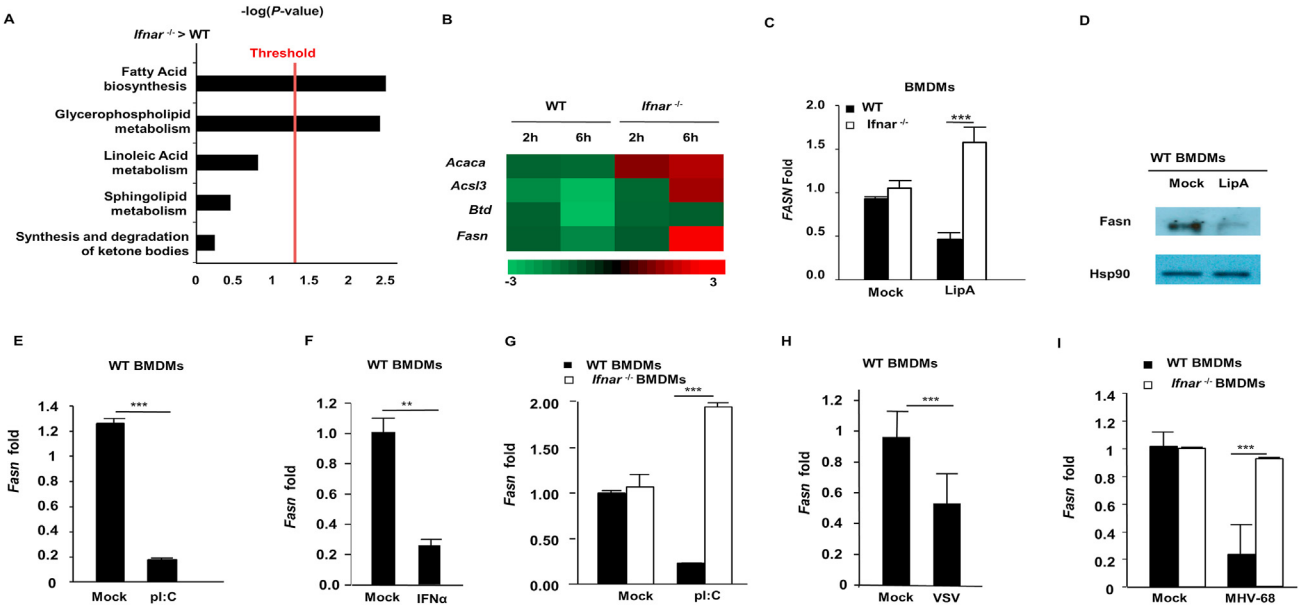

Figure 1 IFN-I downregulates FASN expression through IFNAR/STAT1 pathways. (A) BMDMs isolated from WT or *Ifnar*$^{-/-}$ mice were stimulated with LipA (100 ng/mL) for 6 h and RNA samples were isolated and prepared for RNAseq analysis. Using Ingenuity program, canonical pathways which were differentially modulated in *Ifnar*$^{-/-}$ *vs*. WT BMDMs were identified. (B) Heat map of fold changes in genes significantly modulated in fatty acid biosynthesis based on the RNAseq data. (C) BMDMs derived from WT and *Ifnar*$^{-/-}$ mice stimulated with 200 ng/mL LipA and *Fasn* mRNA levels were assessed by RT-qPCR analysis. (D) WT BMDMs were treated with LipA (200 ng/mL) for 6 h and Fasn protein level was measured by Western blotting. (E) Quantification of *Fasn* mRNA in WT BMDMs treated with 200 ng/mL pI:C by RT-qPCR. (F) WT BMDMs were treated with IFNα (1000 U/mL) for 6 h and *Fasn* mRNA was measured by RT-qPCR. (G) *Fasn* mRNA was quantified in WT and *Ifnar*$^{-/-}$ BMDMs treated with pI:C (200 ng/mL). (H) The level of *Fasn* mRNA was measured in WT BMDMs infected with VSV-GFP (MOI = 1) for 8 h. (I) *Fasn* mRNA was measured in WT and *Ifnar*$^{-/-}$ BMDMs infected with MHV-68 (MOI = 1) for 8 h. Data presented as mean + SD, $n = 3$; $^{**}P < 0.01$, $^{***}P < 0.001$.

PRR stimulation elicit IFN-I (*Ifnβ*/*Ifnα*) gene transcription, and newly synthesized IFN-I signals *via* IFNAR to activate ISGs. Downregulation of *Fasn* requires the synthesis of PRR-induced proteins, as cells treated with the protein translation inhibitor, cycloheximide, failed to reduce *Fasn* gene expression after PRR stimulation, suggesting that FASN may be suppressed in an IFN-I-dependent fashion (Fig. S1D). Indeed, cells treated with recombinant IFN-α displayed a decrease in *Fasn* expression (Fig. 1F). Importantly, and consistent with our RNAseq results, PRR ligand-dependent downregulation of *Fasn* required intact IFNAR and downstream signaling molecules such as STAT1 (Fig. 1G and Fig. S1E). In addition to pure ligands that directly stimulate cytosolic nucleic acid sensing PRRs to induce IFN-I and subsequently suppress FASN, including LipA and pI:C, we examined FASN expression in the context of viral infections. BMDMs infected with vesicular stomatitis virus (VSV), an RNA virus, had a reduction in *Fasn* gene expression compared to uninfected control cells (Fig. 1H). Downregulation of *Fasn* during VSV infection required the detection of viral RNA by host PRRs, as cells lacking either MAVS (also known as IPS-1, Cardif, or VISA, a common adaptor molecule that facilitates IFN-I activation downstream of RNA sensing PRRs), or TLR3 (*Tlr3*$^{-/-}$/*Cardif*$^{-/-}$ double knockout cells) were impaired in their ability to suppress *Fasn* expression (Fig. S1F). Similarly, *Fasn* was downregulated upon infection with DNA viruses, including murine gamma herpes virus 68 (MHV-68) and herpes simplex virus 1 (HSV-1) in an IFNAR-dependent manner (Fig. 1I and Fig. S1G). Taken together, these findings suggest that *Fasn* is downregulated by IFN-I during viral infection.

3.2. *FASN supports a broad range of viral infections*

Our data indicate that FASN is suppressed during viral infections in an IFNAR1-dependent manner, suggesting a possibility that it may be involved in modulating viral infection. To determine the role of FASN in antiviral host defense, we ectopically expressed FASN in HEK 293 T cells before infection with different viruses. Overexpression of FASN resulted in a relative increase of viral loads compared to WT infected cells (Fig. 2A and Supporting Information Fig. S2A). HEK 293 T cells supplemented with palmitate, the downstream product of FASN, also displayed an increase in viral infection in a dose-dependent manner (Fig. 2B). In contrast, knockdown of FASN in HEK 293 T cells by small interfering RNA (siRNA) yielded a reduction of viral loads after infection (Fig. 2C, Fig. S2A and S2B). To further validate the functional role of FASN in promoting virus replication, we generated *FASN*-deficient A549 cells *via* CRISPR technology (Fig. S2C). In agreement with our siRNA knockdown data, cells lacking FASN failed to support viral infection in comparison to WT control cells (Fig. 2D and Fig. S2D).

3.3. *Pharmacological inhibition of FASN restricts viral infections*

C75 (4-methylene-2-octyl-5-oxotetra-hydrofuran-3-carboxylic acid) is a synthetic FASN inhibitor that has been used extensively to study FASN function[43]. We determined the optimal dose for C75 that would not cause cellular toxicity (Fig. S2E). Cellular

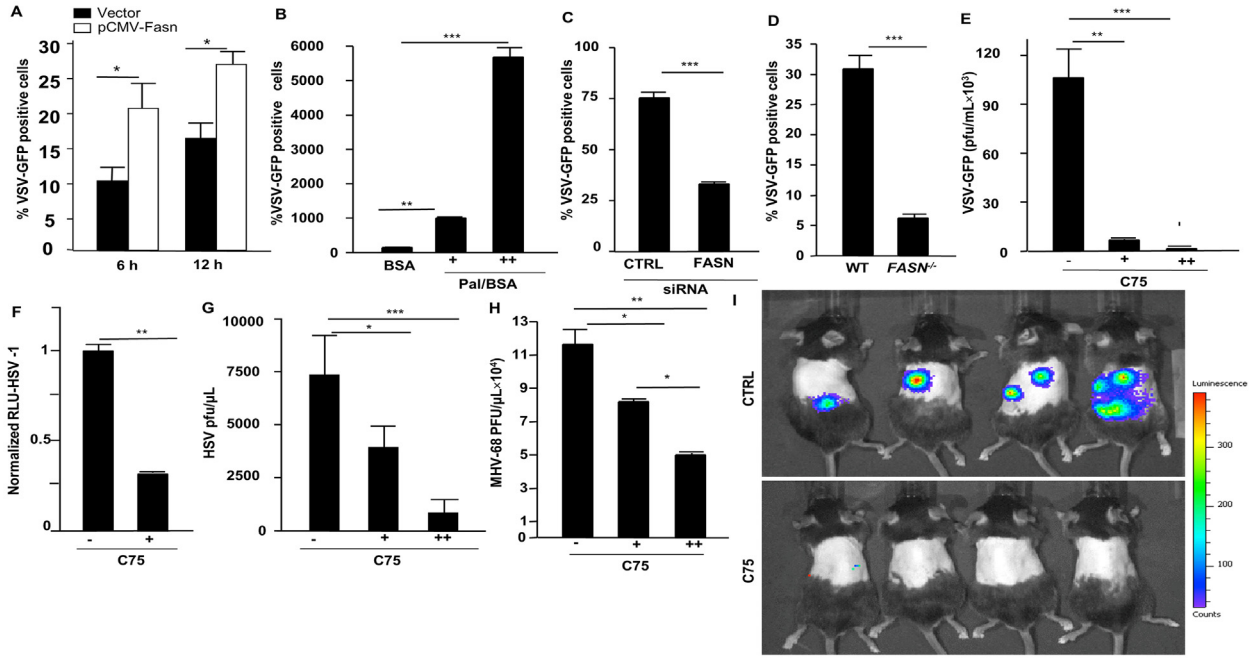

Figure 2 The impact of Fasn expression and activity on viral infection. (A) HEK 293 T cells were transfected with expression plasmids, FASN or control for 36 h prior to VSV infection (MOI = 0.03) and cells were harvested to assess viral infection by FACS. (B) HEK 293 T cells were treated with palmitate/BSA (200 µmol/L) or BSA alone (200 µmol/L) 12 h before VSV infection and cells were harvested at eight hpi for FACS analysis. (C) HEK 293 T cells were transfected with siScramble (control) or siFASN 24 h prior to VSV infection (MOI = 0.03). (D) A549 *Fasn*$^{-/-}$ and WT cells were infected with VSV-GFP (MOI = 0.03) and cells were subjected to FACS analysis. (E) HEK 293 T cells were treated with C75 (5 and 10 µg/mL) for 10 h before VSV-GFP infections. (F) Human monocyte-derived macrophages were treated with C75 for 12 h (5 µg/mL) prior to HSV-1 (expressing luciferase reporter) infection and viral load was measured by luciferase assay. (G) HEK 293 T cells were treated with C75 (5 and 10 µg/mL) for 12 h prior to HSV-1 infections and viral titer was measured by plaque assay. (H) HEK 293 T cells were treated with C75 (5 and 10 µg/mL) for 12 h before MHV68 infections and viral titer was measured by plaque assay (n = 3). (I) Measuring luciferase activity in mice infected with MHV68luc 8 days post-infection with daily administration of C75 (5 mg/kg, i.p.) or DMEM starting 1 day before infection (n = 5). Data presented as mean + SD; *$P < 0.05$, **$P < 0.01$, ***$P < 0.001$, ****$P < 0.0001$.

treatment with C75 significantly reduced both RNA and DNA viruses in HEK 293 T cells and human monocyte-derived macrophages (hPBMC) compared to untreated cells (Fig. 2E−H). To determine whether inhibition of FASN could inhibit viral infection *in vivo*, we administered C75 to mice followed by viral infection and full body imaging analysis. Animals treated with C75 harbored lower viral loads after infection compared to untreated animals (Fig. 2I). Epigallocatechin gallate (EGCG), a catechin found in tea leaves (*Camellia sinensis*)[44], and cerulenin, an antifungal antibiotic and irreversible inhibitor of FASN[45], have both been reported to function as FASN inhibitors. Similar to C75, cellular treatment with EGCG or cerulenin provided protection against a broad range of enveloped viruses (Fig. S2F−S2K). Together, these results demonstrate that C75 and other pharmacological inhibitors of FASN can effectively inhibit viral infections *in vitro* and in *vivo*.

3.4. *FASN facilitates viral entry*

As C75 reduced viral load both *in vitro* and *in vivo*, we wanted to determine the mechanism by which FASN operates to promote viral infection. Interestingly, C75 did not suppress viral infection *via* a mechanism which increases pro-inflammatory or IFN-I cytokines, suggesting that FASN does not function as a steady state negative regulator of the IFN-I response (Supporting Information Fig. S3A). We therefore hypothesized that FASN functions in a manner that does not involve downregulation of innate immune activation pathways, but instead modulates the viral life cycle. Utilizing a pseudo-typed VSV reporter virus (VSVΔG-Luc) that only permits a single round of infection, we infected HEK 293 T cells that were either untreated or treated with the C75 FASN inhibitor. VSVΔG-Luc expression was reduced in cells that were pre-treated with the FASN inhibitor in a dose-dependent manner, indicating that FASN may mediate its pro-viral effects primarily at an early stage in the viral life cycle (Fig. 3A). One of the earliest steps of infection is the attachment of the virus to the host cell membrane. HEK 293 T cells treated with C75, however, showed no significant differences in the number of membrane-attached viral particles when compared to untreated cells, indicating that FASN does not facilitate viral infection at the level of cell membrane attachment (Fig. S3B). We then set out to study the role of FASN on host cell entry, another early step in the viral life cycle. Employing a pseudotyped cytosolic entry reporter VSV-G strain (VSV-G-βlaM), we found that cellular inhibition of FASN *via* C75 or siRNA inhibited the VSV-G-βlaM cytosolic activity, suggesting that FASN mainly supports viral infection by mediating events involved in viral entry (Fig. 3B and Fig. S3C). Indeed, cells ectopically expressing FASN displayed elevated VSV-G-βlaM cytosolic activity compared to control cells (Fig. 3C). Viral entry requires the fusion of viral particles to the host cell membrane in order to achieve infection. For example, fusion (F) and attachment (G) proteins derived from Nipah virus (NiV) induce

pH-independent cell−cell membrane fusion and syncytia formation. Gain of function experiments revealed that FASN enhances membrane fusion and the formation of syncytia between cells (Fig. 3D and E). Alternatively, downregulation of FASN *via* siRNA results in impaired cell−cell membrane fusion and syncytia formation (Fig. 3F and G). These findings reveal a key role for FASN in early viral infection.

3.5. *FASN inhibitors block SARS-CoV-2 replication*

In the setting of the COVID-19 pandemic, we investigated the potential role of FASN in SARS-CoV-2 infection. *FASN* mRNA levels in Hela-ACE-2 (Hela cells constitutively expressing ACE-2) were reduced after IFNα treatment and pI:C transfection. (Supporting Information Fig. S4A and S4B). The *FASN* expression was then measured in Hela-ACE-2 and Huh 7.5 cells infected with SARS-CoV-2. We used the recombinant SARS-CoV-2 expressing mNeonGreen protein (icSARS-CoV-2-mNG), as described by Xie et al., 2020[36]. The *FASN* level was reduced in both cell lines after SARS-CoV-2 infection (Fig. S4C and S4D). To further investigate the role of FASN in this setting, HEK 293 T-ACE2 cells (HEK 293 T cells constitutively expressing ACE2) and Huh 7.5 cells were transfected with siRNA targeting *FASN* and control siRNA (siScramble) for 36 h followed by SARS-CoV-2 infection. The results demonstrated inhibition of viral infection in *FASN*-knockdown cells compared to the cells transfected with control siRNA (Fig. 4A and B and Fig. S4E) in both cell lines. Similarly, overexpression of FASN in Huh 7.5 cells increased the viral load compared to cells transfected with vector alone (Fig. 4C and Fig. S4E). We then tested the effect of the FASN inhibitors on SARS-CoV-2 infection in Huh 7.5, Vero-E6, and Hela-ACE-2 cells. Cells were infected with SARS-CoV-2 and 1 h later were treated with C75, EGCG, Cerulenin, or TVB-3166, an analogue of TVB-2640 which is a selective small molecular inhibitor of FASN[46].

Cells were then harvested and the viral RNA in the cell lysate was quantified by RT-qPCR. Results showed a dose-dependent reduction of SARS-CoV-2 nucleocapsid protein (NP) (Fig. 4D−G). In parallel, infectious viral particles released in the supernatants of the treated cells were measured by standard plaque forming unit assay (PFU) by re-infecting Hela-ACE-2 cells. These results also showed a dose-dependent reduction of viral production in cells treated with the FASN inhibitors (Supporting Information Fig. S5A−S5D).

In addition, we used the mNeonGreen recombinant SARS-CoV-2 to infect Vero-E6 and compared the number of GFP positive cells in the presence or absence of FASN inhibitors using flow cytometric analysis and fluorescent microscopy (Supporting Information Fig. S6). Results showed a dramatic reduction in the number of cells infected with the mNeonGreen recombinant SARS-CoV-2 when comparing cells without treatment (61% infected) to 4.5% infection after C75 and 6.6% after ECGC treatments.

As numerous SARS-CoV-2 variants have appeared since the initial outbreak, we wanted to test whether FASN inhibitors could also effectively suppress infection by these evolved strains, specifically the variants of concern. As shown in Fig. 5, both C75 and TVB-3166 FASN inhibitors suppressed infection by α, β, γ and δ strains at similar efficacies as the WT SARS-CoV-2, based on a viral genomic RNA assay and standard plaque assay (Fig. 5 and Supporting Information Fig. S7). We also obtained similar results with hybrid alphavirus-SARS-CoV-2 pseudo-viruses expressing M, N and E proteins from WT SARS-CoV-2 and S proteins from α, β, γ and δ strains[41] which further suggested that FASN inhibitors effectively inhibited the entry of different SARS-CoV-2 variants (Supporting Information Fig. S8). Overall, our studies have provided evidence that FANS inhibitors have potential to be further

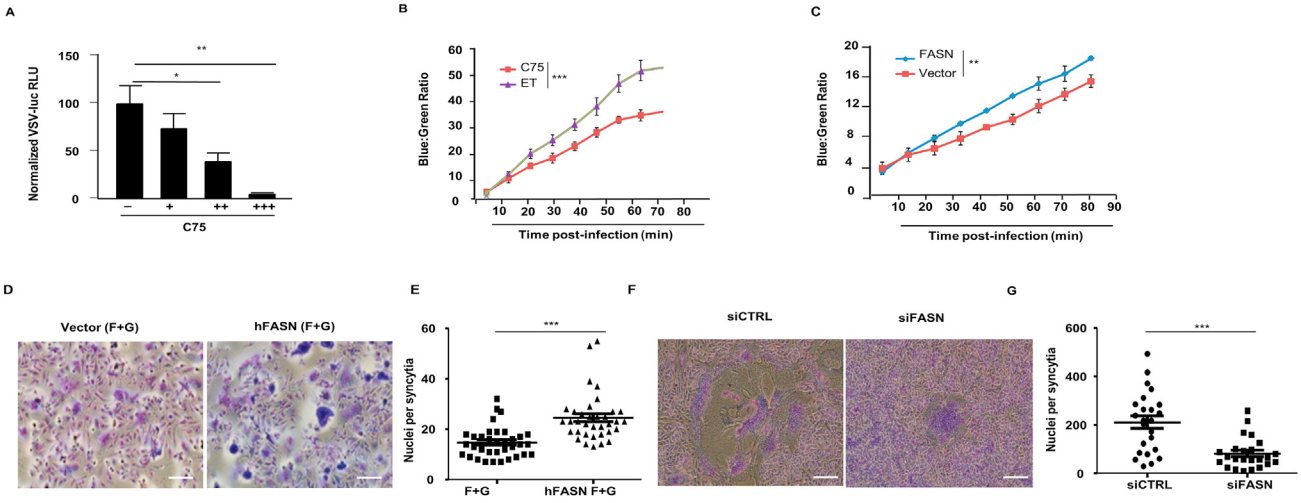

Figure 3 Mechanisms by which modulation of FASN activity affects viral infection. (A) Infection of C75-Pre-treated HEK 293 T cells with replication deficient pseudo-type VSV-renilla luc. (B) HEK 293 T cells were pretreated with C75 (5 μg/mL) or control (ET) for 12 h or (C) transfected with indicated expression plasmids 36 h prior to VSV-G/βlaM infection for 1.5 h. β-Lactamase activity was measured by determining the rate of cleavage of CCF2 (green) to its cleaved form (blue). (D, E) NiV.F/G syncytia assay, Vero cells were transfected with expression plasmids 24 h prior to NiV F and G transfection and formation of syncytia was determined 36 h after F and G transfection. Scale bar = 100 μm. (F, G) Vero cells were transfected with siRNAs 24 h prior to NiV F and G transfection as well as another round of siRNA transfection. Cells were fixed and syncytia formation was determined 60 h post F and G transfection (n = 3). Scale bar = 100 μm. Data presented as mean + SD; $^*P < 0.05$, $^{**}P < 0.01$, $^{***}P < 0.001$.

developed into broad spectrum antiviral agents against multiple viruses, including emerging viruses such as SARS-CoV-2.

3.6. *Identification of CC_{50} and IC_{50} values for FASN inhibitors*

To determine the potential cytotoxic effect of the compounds used in our study, the 50% cytotoxic concentration (CC_{50}) was evaluated by treating different cell types with 2-fold serial dilutions of C75, cerulenin, and TVB-3166 for 18 h (Supporting Information Fig. S9A−S9I).

We did not detect any apparent cytotoxicity with concentrations of the compounds used to inhibit viral infection in this study. The concentrations used to inhibit 50% of viral infection (IC_{50}) was determined for C75, EGCG, cerulenin, and TVB-3166 by infecting cells with SARS-CoV-2 followed by treating cells with the FASN inhibitors for about 20−24 h (Supporting Information Fig. S10A−S10E). The IC_{50} for C75 was about 1.6−2 μmol/L, the CC_{50} was 12−23, 19, and 33.6 μmol/L for Hela-ACE-2, Huh 7.5 and Vero-E6, respectively. The IC_{50} of EGCG was 2.7−3.4 μmol/L. Cerulenin IC_{50} was 1.4−2.2 μmol/L, and its CC_{50} was 10.7, 25.7−28, and 26.7−33 μmol/L for Hela-ACE-2, Huh 7.5 and Vero-E6, respectively. The TVB IC_{50} was 9.5−10.35 μmol/L and the CC_{50} was 39.8−44.3, 51.8−64, and 57.2−80.4 μmol/L for Hela-ACE-2, Huh 7.5 and Vero-E6, respectively.

Therefore, the effective dose for viral inhibition for the FASN inhibitors in this study was much smaller than the CC_{50}. However, at higher concentrations there was an apparent toxicity for these inhibitors of FASN (Fig. S9A−S9I).

4. Discussion

Viruses rely on the metabolic network of the host cell, commandeering nucleotide biosynthetic pathways as well as glucose and lipid metabolic pathways to fuel their replication. Some viruses even alter the host's cellular metabolism to favor their own life cycle. For instance, human cytomegalovirus (HCMV) infection upregulates fatty acid biosynthesis and glycolysis, while herpes simplex virus-1 (HSV-1) appears to inhibit glycolytic flux and directs host metabolic pathways towards enhanced pyrimidine synthesis[47,48]. The efficiency of HCV assembly is mainly determined by the droplet-binding domain of the HCV core protein[49]. Additionally, recent studies suggest that both Kaposi's sarcoma-associated herpes virus (KSHV) and West Nile virus (WNV) induce lipogenesis[50,51] and long term lipid metabolism alteration has also been documented in patients recovered from SARS-CoV-1[52]. We have shown that over-expression of FASN facilitates viral infection, whereas knockout or knockdown of FASN inhibits it. The role of FASN in promoting the replication of many RNA and DNA viruses, including human cytomegalovirus (HCMV)[23], Kaposi sarcoma-associated herpesvirus (KSHV)[24], cytomegalovirus (CMV)[23], dengue virus (DENV)[26], chikungunya virus (CHIKV)[28], and HIV and HCV[30,31] has been previously studied.

While viruses have evolved to alter specific host metabolic pathways, it is unclear whether or how host cells alter their own metabolism to protect themselves from viral infection. Innate antiviral immunity operates *via* an IFNAR dependent manner, where IFN-I induction triggers the activation of a JAK−STAT

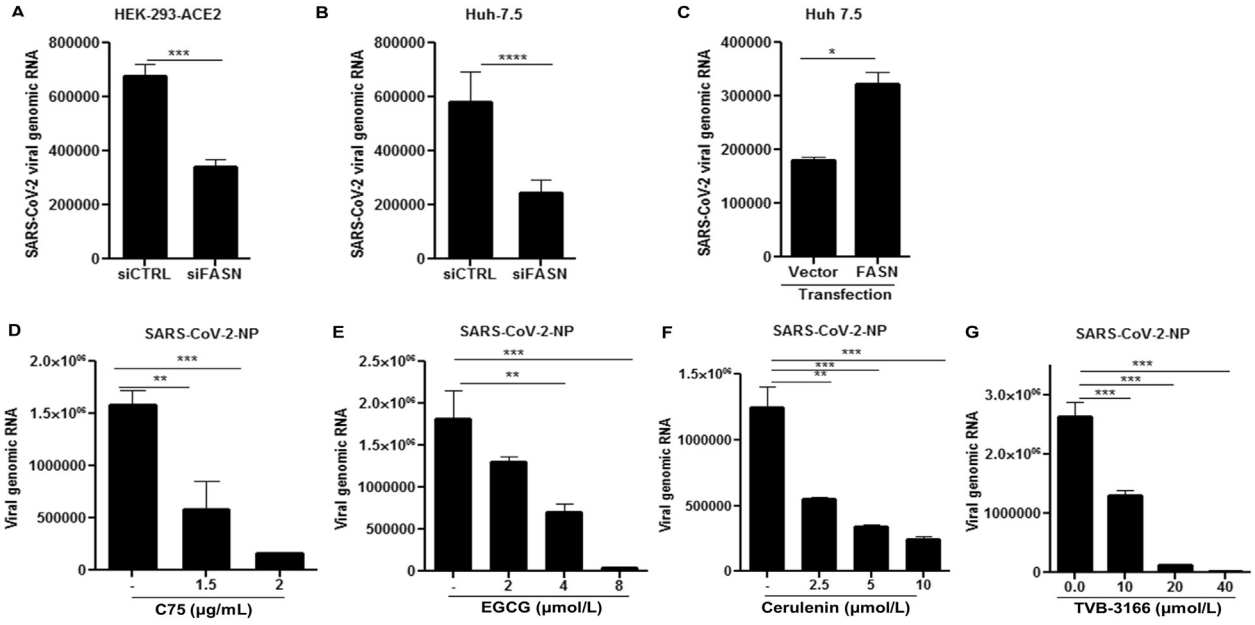

Figure 4 SARS-CoV-2 replication can be inhibited by downregulation of FASN. (A) HEK-293 T-ACE2 and (B) Huh 7.5 cells were transfected with siRNA targeting FASN or scramble siRNA (siCTRL) followed by SARS-CoV-2 infection at MOI of 0.01. (C) Transfection of Huh-7.5 cells with a vector expressing FASN or vector alone followed by SARS-CoV-2 infection. (D−G) Huh-7.5 cells were treated with indicated dose of C75, EGCG, cerulenin, and TVB-3166 1 h post SARS-CoV-2 infection. The supernatant was used for titrating the viral RNA copy number and plaque assay. The cell lysate was subjected to RNA extraction to evaluate the viral RNA transcripts by using RT-qPCR ($n = 3$). All data are means ± SEM; $^{**}P < 0.01$, $^{***}P < 0.001$, $^{****}P < 0.0001$.

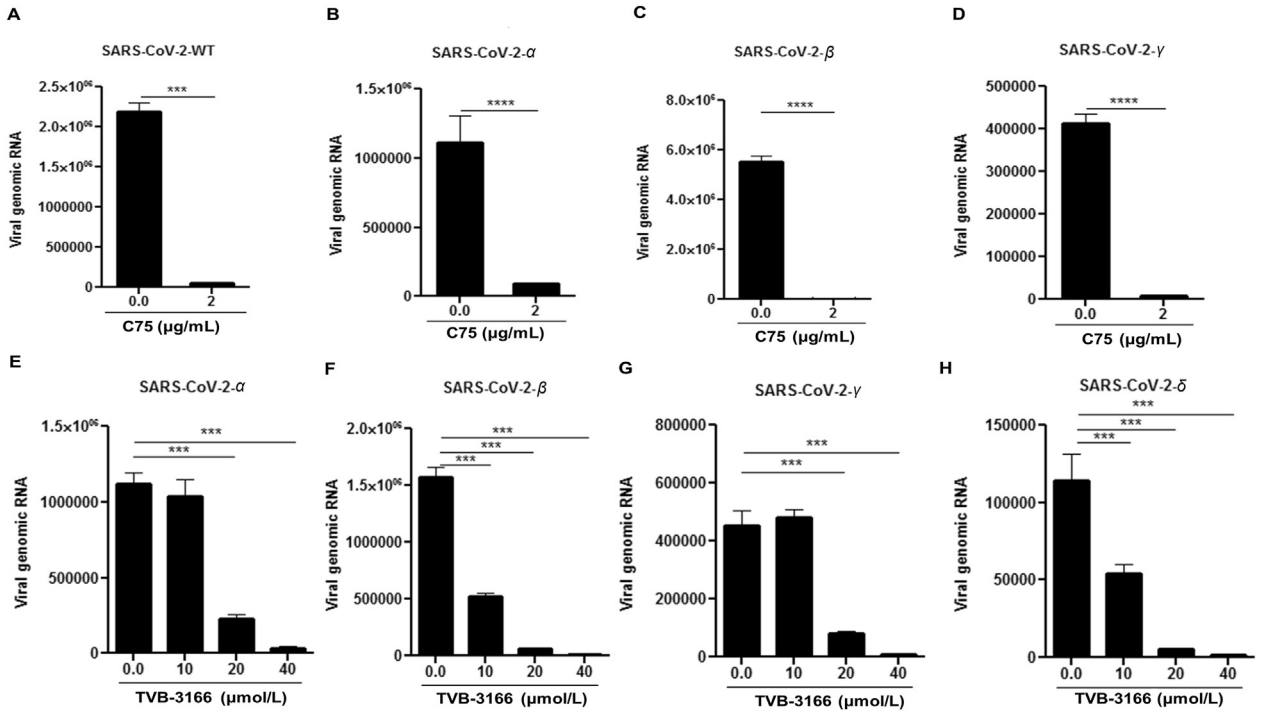

Figure 5 SARS-CoV-2 variants of concern can be inhibited by FASN inhibitors. The Huh 7.5 cells were infected with (A) SARS-CoV-2-WT, (B) SARS-CoV-2-α, (C) SARS-CoV-2-β and (D) SARS-CoV-2-γ at MOI of 0.01 and treated with 2 μg/mL C75 1 h post infection. The Hela-ACE-2 cells were infected with (E) SARS-CoV-2-α, (F) SARS-CoV-2-β, (G) SARS-CoV-2-γ, and (H) SARS-CoV-2-δ at MOI of 0.01 and treated with TVB-3166 at indicated dose 1 h post infection. The cell lysate was harvested for measuring the viral RNA transcripts by using RT-qPCR 24 h post-infection ($n = 3$). All data are means ± SEM; ***$P < 0.001$, ****$P < 0.0001$.

pathway resulting in the formation of the STAT1−STAT2−IRF9 transcription factor complex, which binds to interferon stimulatory response elements (ISRE) on ISGs to positively drive their transcription[53,54]. It is believed that innate antiviral immunity is mainly mediated *via* IFN-I-dependent induction of ISGs, which collectively foster an antiviral state. We and others have previously identified numerous antiviral genes by screening through hundreds of ISGs[19,20,55]. In this report, we have demonstrated that *Fasn* is downregulated in response to not only LPS and pI:C stimulations, but also by different viral infections. Our results have further shown that *Fasn* is suppressed not only in an IFNAR-dependent manner, but also in a STAT1-dependent manner. How the STAT1 transcription factor functions to suppress *Fasn* gene transcription is unknown and is currently under investigation. More importantly, our studies suggest that the mechanism by which IFN-I downregulates certain metabolic genes includes commandeering part of the innate immune antiviral program.

Fatty acids are essential molecules in cell membranes, membranous organelles, signaling, and energy storage. FASN catalyzes the synthesis of palmitate (C16:0), a long chain fatty acid that influences the physical properties of the cell by modulating the fluidity of membrane lipid bilayers. FASN deficiency leads to changes in the composition of the cell membrane[33]. Viral infection requires optimal membrane fluidity, which leads to the clustering of receptors for cell entry[56−58]. We have shown that FASN inhibitors suppress viral entry by blocking fusion between viral and cellular membranes. Additionally, downregulation of FASN by siRNA results in decreasing the viral infection rate, though not as pronounced as that of the pharmacological inhibitors of FASN. The difference may be due to limitations in our study for transient transfection in different cell types, or because of possible off target effects of FASN inhibitors. We have also found that FASN inhibitors can suppress cell−cell membrane fusion and syncytia formation driven by viral proteins, impacting viral infection in multiple stages of the viral life cycle. The results of this study highlight the promising antiviral potency of FASN inhibitors, and their potential role in developing novel antiviral therapeutics. Interestingly, certain viruses co-opt host palmitoyltransferases to modify viral proteins to support optimal infection[59]. These enzymes regulate palmitoylation (aka *S*-acylation), a post-translational modification yielding the covalent linkage of palmitate to cysteine residues, which often results in proteins associating with cell membranes[60,61]. In addition, palmitoylation of the Spike protein is a common strategy for coronaviruses, including SARS-CoV-1 and SARS-CoV-2, to facilitate membrane trafficking and reaching optimal infectivity[62]. Our data also showed that exogenous palmitate supports viral infection. It is therefore possible that inhibition of FASN could restrict viral infection at multiple levels, including entry as well as viral protein-host membrane interactions. However, future studies are necessary to fully elucidate the mechanisms responsible for the function of FASN in viral entry and other steps in the viral life cycle.

More importantly, our studies indicate that FASN inhibitors can act as broad antiviral agents against different types of viruses, including VSV, HSV-1, MHV68 and especially emerging infectious viruses such as SARS-CoV-2. Many antiviral drugs target specific viral proteins such as the HIV reverse transcriptase or influenza neuraminidase, which have been developed over years of study against such long existing viruses. However, in the

past two decades, we have been challenged with numerous emerging and highly pathogenic viruses, including SARS, MERS, Ebola, Zika and SARS-CoV-2. We are still learning about the pathogenesis of these viruses, and we do not always have the luxury of waiting for decades of research to show us the optimal drug targets. Agents that apply broadly-acting antiviral strategies could potentially be used as first line agents against novel diseases caused by many different types of viruses. We previously demonstrated that 25-hydroxycholesterol (25HC), the metabolic product of the IFN-I inducible cholesterol 25-hydroxylase, is a broad-spectrum antiviral agent against numerous types of viruses, including SARS-CoV-2[63]. In this manuscript, we provide evidence that inhibitors of FASN can also be used as broad-spectrum antiviral agents. In particular, we have shown that multiple FASN inhibitors, including C75, EGCG, Cerulenin and TVB-3166, could strongly suppress SARS-CoV-2 infection. Additionally, downregulation or knockdown of *Fasn* also results in inhibiting SARS-CoV-2 infection. We have also provided evidence suggesting that the FASN inhibitors can suppress infection by different SARS-CoV-2 variants, including α, β, γ and δ SARS-CoV-2 at a similar efficacy as the WT SARS-CoV-2.

Interestingly, AM-580, an inhibitor of sterol regulatory element binding protein-1 (SREBP-1) has been shown to have antiviral properties against MERS-CoV in Huh7.5 cells[64]. We have previously shown that SARS-CoV-2 stabilizes the SREBP-1 by protease cleavage of IFN-I inducible gene, ring finger protein 20 (RNF-20) for optimum infection[65]. Thus, future studies should explore the role of SREBP-1 inhibition on viral infection through regulation of its downstream gene, FASN. We have shown that IFN-I downregulates FASN as a defense mechanism against wide range of enveloped viruses. Overall, our findings uncover a novel mechanism for IFN-I in host defense against viral infection by suppressing FASN, which catalyzes fatty acid synthesis. Besides *Fasn*, we found that other lipid metabolic genes such as *Acaca* and *Acsl3* are also suppressed by IFN-I. As all viruses take advantage of host metabolic products for their rapid growth, suppressing host metabolic genes might be a general and effective strategy to control viral growth. Further studies in the cross-talk between innate immune pathways and host metabolisms may provide new insights in developing broad spectrum antiviral agents against different types of viral infections and resulting diseases like COVID-19.

5. Conclusions

Viruses reprogram the cellular metabolism of the host cell for optimal growth. The host innate immune signaling pathway counteracts viral invasion by inducing type-I-interferon (IFN-I). Subsequently, IFN-I up-/downregulates expression of particular genes to block viral infection. Fatty acid synthase (FASN), the sole enzyme involved in de novo fatty acid synthesis is downregulated possibly by IFN-I upon viral infection. We have shown that FASN deficiency or suppression by pharmacological inhibitors including C75, cerulenin, EGCG, and TVB-3166 significantly blocks replication and spread of a wide variety of enveloped viruses including SARS-CoV-2 and its variants of concern. As viruses rely entirely on host cell's molecular machinery and metabolic products for adequate growth, suppressing host metabolic genes might be a general and effective strategy to fight against novel diseases caused by many different types of viruses.

Acknowledgments

This project is supported by the Research Funds from US National Institute of Health funds (AI069120, AI158154, and AI149718), the UCLA AIDS Institute and UCLA David Geffen School of Medicine—Eli and Edythe Broad Center of Regenerative Medicine and Stem Cell Research Award Program and Tumor Immunology Training Grant (T32CA912036A1, USA). We thank Dr. Vaithilingarajai Arumugaswami at UCLA for sharing the SARS-CoV-2 variants of concerns obtained from the BEI resources. We thank Ms. Barbara Dillon, the director of the UCLA BSL3 facility for providing a safe and organized laboratory for performing the SARS-CoV-2-based research projects.

Author contributions

Saba R. Aliyari and Amir Ali Ghaffari contributed equally in the design of the study and writing of this manuscript. Amir Ali Ghaffari started the project and was joined later with Saba R. Aliyari in the design and execution of the majority of the experiments. Olivier Pernet in Benhur Lee lab assisted in the design and performance of membrane fusion studies and with Armin Takallou and Adele Zhang generated CRISPR-based FASN knockout cells. Kislay Parvatiyar assisted with experimental design. Clay F. Semenkovich, and Xiaochao Wei assisted with generating LysM-*Fasn* mice. Karen Reue and Laurent Vergnes provided reagents and valuable expertise in metabolism. Linda D. Chilin and Yuntao Wu designed and performed the Ha-CoV-2 pseudo-virus inhibition assays. Ann-Jay Tong from Stephen Smale laboratory contributed to the performance of RNAseq. Yao Wang and Hoda Gerami assisted in performing gene regulation studies and all authors read and approved the manuscript. Genhong Cheng is involved in overall project design and manuscript preparation.

Conflicts of interest

The authors declare no conflicts of interest.

Appendix A. Supporting information

Supporting data to this article can be found online at https://doi.org/10.1016/j.apsb.2022.02.019.

References

1. Cui J, Li F, Shi ZL. Origin and evolution of pathogenic coronaviruses. *Nat Rev Microbiol* 2019;**17**:181–92.
2. V'Kovski P, Kratzel A, Steiner S, Stalder H, Thiel V. Coronavirus biology and replication: implications for SARS-CoV-2. *Nat Rev Microbiol* 2021;**19**:155–70.
3. WHO. https://www.Who.Int/Emergencies/Diseases/Novel-Coronavirus-2019.
4. Henderson LA, Canna SW, Friedman KG, Gorelik M, Lapidus SK, Bassiri H, et al. American college of rheumatology clinical guidance for multisystem inflammatory syndrome in children associated with SARS-CoV-2 and hyperinflammation in pediatric COVID-19: version 2. *Arthritis Rheumatol* 2021;**73**:e13–29.
5. Akira S. Pathogen recognition by innate immunity and its signaling. *Proc Jpn Acad Ser B Phys Biol Sci* 2009;**85**:143–56.
6. Fensterl V, Sen GC. Interferons and viral infections. *Biofactors* 2009;**35**:14–20.

7. Janeway Jr CA, Medzhitov R. Innate immune recognition. *Annu Rev Immunol* 2002;**20**:197−216.
8. Meylan E, Tschopp J, Karin M. Intracellular pattern recognition receptors in the host response. *Nature* 2006;**442**:39−44.
9. Seth RB, Sun L, Chen ZJ. Antiviral innate immunity pathways. *Cell Res* 2006;**16**:141−7.
10. Akira S, Takeda K. Toll-like receptor signalling. *Nat Rev Immunol* 2004;**4**:499−511.
11. Ishikawa H, Barber GN. Sting is an endoplasmic reticulum adaptor that facilitates innate immune signalling. *Nature* 2008;**455**:674−8.
12. Sun L, Wu J, Du F, Chen X, Chen ZJ. Cyclic GMP−AMP synthase is a cytosolic DNA sensor that activates the type I interferon pathway. *Science* 2013;**339**:786−91.
13. Kawai T, Akira S. Antiviral signaling through pattern recognition receptors. *J Biochem* 2007;**141**:137−45.
14. Toshchakov V, Jones BW, Perera PY, Thomas K, Cody MJ, Zhang S, et al. TLR4, but not TLR2, mediates IFN-beta-induced STAT1alpha/beta-dependent gene expression in macrophages. *Nat Immunol* 2002;**3**:392−8.
15. Kawai T, Akira S. The role of pattern-recognition receptors in innate immunity: update on Toll-like receptors. *Nat Immunol* 2010;**11**:373−84.
16. Chelbi-Alix MK, Wietzerbin J. Interferon, a growing cytokine family: 50 years of interferon research. *Biochimie* 2007;**89**:713−8.
17. Le Page C, Génin P, Baines MG, Hiscott J. Interferon activation and innate immunity. *Rev Immunogenet* 2000;**2**:374−86.
18. Schoggins JW, Wilson SJ, Panis M, Murphy MY, Jones CT, Bieniasz P, et al. A diverse range of gene products are effectors of the type I interferon antiviral response. *Nature* 2011;**472**:481−5.
19. Liu SY, Sanchez DJ, Aliyari R, Lu S, Cheng G. Systematic identification of type I and type II interferon-induced antiviral factors. *Proc Natl Acad Sci U S A* 2012;**109**:4239−44.
20. Liu SY, Aliyari R, Chikere K, Li G, Marsden MD, Smith JK, et al. Interferon-inducible cholesterol-25-hydroxylase broadly inhibits viral entry by production of 25-hydroxycholesterol. *Immunity* 2013;**38**:92−105.
21. Der SD, Zhou A, Williams BR, Silverman RH. Identification of genes differentially regulated by interferon alpha, beta, or gamma using oligonucleotide arrays. *Proc Natl Acad Sci U S A* 1998;**95**:15623−8.
22. Megger DA, Philipp J, Le-Trilling VTK, Sitek B, Trilling M. Deciphering of the human interferon-regulated proteome by mass spectrometry-based quantitative analysis reveals extent and dynamics of protein induction and repression. *Front Immunol* 2017;**8**:1139.
23. Spencer CM, Schafer XL, Moorman NJ, Munger J. Human cytomegalovirus induces the activity and expression of acetyl-coenzyme a carboxylase, a fatty acid biosynthetic enzyme whose inhibition attenuates viral replication. *J Virol* 2011;**85**:5814−24.
24. Sanchez EL, Pulliam TH, Dimaio TA, Thalhofer AB, Delgado T, Lagunoff M. Glycolysis, glutaminolysis, and fatty acid synthesis are required for distinct stages of Kaposi's sarcoma-associated herpesvirus lytic replication. *J Virol* 2017;**91**:e02237-16.
25. Heaton NS, Perera R, Berger KL, Khadka S, Lacount DJ, Kuhn RJ, et al. Dengue virus nonstructural protein 3 redistributes fatty acid synthase to sites of viral replication and increases cellular fatty acid synthesis. *Proc Natl Acad Sci U S A* 2010;**107**:17345−50.
26. Tongluan N, Ramphan S, Wintachai P, Jaresitthikunchai J, Khongwichit S, Wikan N, et al. Involvement of fatty acid synthase in Dengue virus infection. *Virol J* 2017;**14**:28.
27. Tang WC, Lin RJ, Liao CL, Lin YL. Rab 18 facilitates dengue virus infection by targeting fatty acid synthase to sites of viral replication. *J Virol* 2014;**88**:6793−804.
28. Zhang N, Zhao H, Zhang L. Fatty acid synthase promotes the palmitoylation of chikungunya virus NSP1. *J Virol* 2019;**93**:e01747-18.
29. Gaunt ER, Cheung W, Richards JE, Lever A, Desselberger U. Inhibition of rotavirus replication by downregulation of fatty acid synthesis. *J Gen Virol* 2013;**94**:1310−7.
30. Aragonès G, Alonso-Villaverde C, Oliveras-Ferraros C, Beltrán-Debón R, Rull A, Rodríguez-Sanabria F, et al. Infection with HIV and HCV enhances the release of fatty acid synthase into circulation: evidence for a novel indicator of viral infection. *BMC Gastroenterol* 2010;**10**:92.
31. Huang JT, Tseng CP, Liao MH, Lu SC, Yeh WZ, Sakamoto N, et al. Hepatitis C virus replication is modulated by the interaction of nonstructural protein NS5B and fatty acid synthase. *J Virol* 2013;**87**:4994−5004.
32. Yang W, Hood BL, Chadwick SL, Liu S, Watkins SC, Luo G, et al. Fatty acid synthase is up-regulated during hepatitis C virus infection and regulates hepatitis C virus entry and production. *Hepatology* 2008;**48**:1396−403.
33. Wei X, Song H, Yin L, Rizzo MG, Sidhu R, Covey DF, et al. Fatty acid synthesis configures the plasma membrane for inflammation in diabetes. *Nature* 2016;**539**:294−8.
34. Tian X, Xu F, Lung WY, Meyerson C, Ghaffari AA, Cheng G, et al. Poly I:C enhances susceptibility to secondary pulmonary infections by Gram-positive bacteria. *PLoS One* 2012;**7**:e41879.
35. Li Y, Wang S, Zhu H, Zheng C. Cloning of the herpes simplex virus type 1 genome as a novel luciferase-tagged infectious bacterial artificial chromosome. *Arch Virol* 2011;**156**:2267−72.
36. Xie X, Muruato A, Lokugamage KG, Narayanan K, Zhang X, Zou J, et al. An infectious cDNA clone of SARS-CoV-2. *Cell Host Microbe* 2020;**27**:841−848.e3.
37. Bhatt AP, Jacobs SR, Freemerman AJ, Makowski L, Rathmell JC, Dittmer DP, et al. Dysregulation of fatty acid synthesis and glycolysis in non-Hodgkin lymphoma. *Proc Natl Acad Sci U S A* 2012;**109**:11818−23.
38. Levin JZ, Yassour M, Adiconis X, Nusbaum C, Thompson DA, Friedman N, et al. Comprehensive comparative analysis of strand-specific RNA sequencing methods. *Nat Methods* 2010;**7**:709−15.
39. Trapnell C, Pachter L, Salzberg SL. Tophat: discovering splice junctions with RNA-Seq. *Bioinformatics* 2009;**25**:1105−11.
40. Takada A, Robison C, Goto H, Sanchez A, Murti KG, Whitt MA, et al. A system for functional analysis of Ebola virus glycoprotein. *Proc Natl Acad Sci U S A* 1997;**94**:14764−9.
41. Hetrick B, He S, Chilin LD, Dabbagh D, Alem F, Narayanan A, et al. Development of a novel hybrid alphavirus-SARS-CoV-2 particle for rapid *in vitro* screening and quantification of neutralization antibodies, antiviral drugs, and viral mutations. *bioRxive* 2021. Available from https://doi.org/10.1101/2020.12.22.423965.
42. Wolf MC, Wang Y, Freiberg AN, Aguilar HC, Holbrook MR, Lee B. A catalytically and genetically optimized beta-lactamase-matrix based assay for sensitive, specific, and higher throughput analysis of native henipavirus entry characteristics. *Virol J* 2009;**6**:119.
43. Kuhajda FP, Pizer ES, Li JN, Mani NS, Frehywot GL, Townsend CA. Synthesis and antitumor activity of an inhibitor of fatty acid synthase. *Proc Natl Acad Sci U S A* 2000;**97**:3450−4.
44. Tian WX. Inhibition of fatty acid synthase by polyphenols. *Curr Med Chem* 2006;**13**:967−77.
45. Deepa PR, Vandhana S, Muthukumaran S, Umashankar V, Jayanthi U, Krishnakumar S. Chemical inhibition of fatty acid synthase: molecular docking analysis and biochemical validation in ocular cancer cells. *J Ocul Biol Dis Inf* 2010;**3**:117−28.
46. Falchook G, Infante J, Arkenau HT, Patel MR, Dean E, Borazanci E, et al. First-in-human study of the safety, pharmacokinetics, and pharmacodynamics of first-in-class fatty acid synthase inhibitor TVB-2640 alone and with a taxane in advanced tumors. *EClinicalMedicine* 2021;**34**:100797.
47. Munger J, Bennett BD, Parikh A, Feng XJ, McArdle J, Rabitz HA, et al. Systems-level metabolic flux profiling identifies fatty acid synthesis as a target for antiviral therapy. *Nat Biotechnol* 2008;**26**:1179−86.
48. Vastag L, Koyuncu E, Grady SL, Shenk TE, Rabinowitz JD. Divergent effects of human cytomegalovirus and herpes simplex virus-1 on cellular metabolism. *PLoS Pathog* 2011;**7**:e1002124.
49. Shavinskaya A, Boulant S, Penin F, McLauchlan J, Bartenschlager R. The lipid droplet binding domain of hepatitis C virus core protein is a major

determinant for efficient virus assembly. *J Biol Chem* 2007;**282**:37158−69.
50. Delgado T, Sanchez EL, Camarda R, Lagunoff M. Global metabolic profiling of infection by an oncogenic virus: KSHV induces and requires lipogenesis for survival of latent infection. *PLoS Pathog* 2012;**8**:e1002866.
51. Martín-Acebes MA, Blázquez AB, Jiménez de Oya N, Escribano-Romero E, Saiz JC. West Nile virus replication requires fatty acid synthesis but is independent on phosphatidylinositol-4-phosphate lipids. *PLoS One* 2011;**6**:e24970.
52. Wu Q, Zhou L, Sun X, Yan Z, Hu C, Wu J, et al. Altered lipid metabolism in recovered sars patients twelve years after infection. *Sci Rep* 2017;**7**:9110.
53. Ghislain JJ, Wong T, Nguyen M, Fish EN. The interferon-inducible STAT2:STAT1 heterodimer preferentially binds *in vitro* to a consensus element found in the promoters of a subset of interferon-stimulated genes. *J Interferon Cytokine Res* 2001;**21**:379−88.
54. Wesoly J, Szweykowska-Kulinska Z, Bluyssen HA. STAT activation and differential complex formation dictate selectivity of interferon responses. *Acta Biochim Pol* 2007;**54**:27−38.
55. Li C, Deng YQ, Wang S, Ma F, Aliyari R, Huang XY, et al. 25-Hydroxycholesterol protects host against Zika virus infection and its associated microcephaly in a mouse model. *Immunity* 2017;**46**:446−56.
56. de Armas-Rillo L, Valera MS, Marrero-Hernández S, Valenzuela-Fernández A. Membrane dynamics associated with viral infection. *Rev Med Virol* 2016;**26**:146−60.
57. Heaton NS, Randall G. Multifaceted roles for lipids in viral infection. *Trends Microbiol* 2011;**19**:368−75.
58. Mazzon M, Mercer J. Lipid interactions during virus entry and infection. *Cell Microbiol* 2014;**16**:1493−502.
59. Gouttenoire J, Pollán A, Abrami L, Oechslin N, Mauron J, Matter M, et al. Palmitoylation mediates membrane association of hepatitis E virus ORF3 protein and is required for infectious particle secretion. *PLoS Pathog* 2018;**14**:e1007471.
60. Kadoshima T, Sakaguchi H, Nakano T, Soen M, Ando S, Eiraku M, et al. Self-organization of axial polarity, inside-out layer pattern, and species-specific progenitor dynamics in human ES cell-derived neocortex. *Proc Natl Acad Sci U S A* 2013;**110**:20284−9.
61. Sobocińska J, Roszczenko-Jasińska P, Ciesielska A, Kwiatkowska K. Protein palmitoylation and its role in bacterial and viral infections. *Front Immunol* 2017;**8**:2003.
62. Wu Z, Zhang Z, Wang X, Zhang J, Ren C, Li Y, et al. Palmitoylation of SARS-CoV-2 S protein is essential for viral infectivity. *Signal Transduct Target Ther* 2021;**6**:231.
63. Zu S, Deng YQ, Zhou C, Li J, Li L, Chen Q, et al. 25-Hydroxycholesterol is a potent SARS-CoV-2 inhibitor. *Cell Res* 2020;**30**:1043−5.
64. Yuan S, Chu H, Chan JF, Ye ZW, Wen L, Yan B, et al. Srebp-dependent lipidomic reprogramming as a broad-spectrum antiviral target. *Nat Commun* 2019;**10**:120.
65. Zhang S, Wang J, Cheng G. Protease cleavage of RNF20 facilitates coronavirus replication *via* stabilization of SREBP1. *Proc Natl Acad Sci U S A* 2021;**118**:e2107108118.